IEEE Access
Multidisciplinary | Rapid Review | Open Access Journal

Received August 19, 2020, accepted August 21, 2020, date of publication August 24, 2020, date of current version September 4, 2020.

Digital Object Identifier 10.1109/ACCESS.2020.3019174

A Scalable Ka-Band 1024-Element Transmit Dual-Circularly-Polarized Planar Phased Array for SATCOM Application

XUAN LUO[1], (Associate Member, IEEE), JUN OUYANG[1], ZHI-HUI CHEN[2], YI YAN[1], (Member, IEEE), LEI HAN[3], ZUBING WU[2], TAO YU[2], AND KAI ZHENG[2]

[1]School of Electronic Science and Engineering, University of Electronic Science and Technology of China (UESTC), Chengdu 611731, China
[2]Chengdu T-Ray Technology Company Ltd., Chengdu 610041, China
[3]Air and Missile Defense College Institute, Air Force Engineering University, Xi'an 710051, China

Corresponding author: Jun Ouyang (yjou@uestc.edu.cn)

ABSTRACT This paper presents a scalable 1024-element transmit dual-circularly-polarized phased array for Ka-band satellite communication (SATCOM) terminal applications. The transmit array based on the CMOS beamformer and a multilayer printed circuit board (PCB) can steer up to large scan angles (±60°) with a scan loss less than 4.5 dB. With the 8-channel transmit beamformer, the array can realize dual circular polarization and the axial ratio (AR) of the array is less than 3 dB in the scanning range of ±30° in both left-hand circular polarization (LHCP) and right-hand circular polarization (RHCP) mode. The effective isotropic radiated power (EIRP) of the array achieves 74 dBm from 29.5 GHz to 30 GHz. The design and measurement of the 1024-element transmit array have presented a feasible way for mass production of a low cost active phased array.

INDEX TERMS Ka-band, SATCOM, phased array, flat panel antenna, CMOS, dual-circularly-polarized.

I. INTRODUCTION

With the development of the high throughput satellite (HTS) systems and low earth orbiting satellite (LEO) systems [1]–[4], SATCOM operators can provide low price and global coverage. Therefore, the number of SATCOM users has significantly increased in recent years. Meanwhile, SATCOM users increasingly demand satellite terminals with a low profile, rapid beam steering and high reliability. However, the traditional SATCOM terminals applying mechanically steered antennas are bulky and not reliable for long-term use. Mass production of beam-steering antenna for SATCOM terminals of the LEO system is the most urgent technological advancement.

In recent years, researchers have proposed different solutions to realize the beam-steering antenna. The transmit array and reflect array [5]–[7] can achieve beam steering with very low cost. However, the phase-delay and phase-rotation cell of the transmit array and reflect array require mechanical manufacturing with high accuracy. Furthermore, due to the restriction of the ratio of focal length to diameter (F/D), the transmit array and reflect array are difficult to make low profile. Others have found that a liquid crystal performed as a tunable dielectric material can be used to substitute the phase shifters in phased arrays [8], [9]. They have demonstrated that an electronically scanned antenna based on a liquid crystal is low profile and can achieve a wide-angle scan (±60°). Due to the ease of production of liquid crystals, this technology is also low cost. However, the insertion loss of the device based on liquid crystals is high, especially in millimeter-wave frequencies. The measured gain of a 2 × 2 array introduced by [9] at 17.5GHz is only 5.9 dBi. With the increase in the aperture of the array, the insertion loss of the feed network can significantly undermine the performance of the array. Furthermore, the liquid crystal is sensitive to temperature, so it is not suitable for platforms operating in extreme temperature, such as airborne systems.

The active phased array is one of the most feasible technologies for SATCOM terminal applications. The phased array can steer the beam at high speed with high reliability. Moreover, compared with the EIRP of a single element, the EIRP of an N-element transmit improves by N^2 [10]. Therefore, it is efficient for the transmit array to achieve high EIRP. From current reports [10-23], the silicon-based

The associate editor coordinating the review of this manuscript and approving it for publication was Giorgio Montisci.

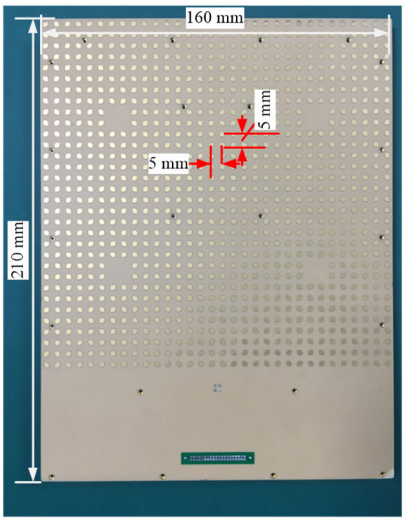

(a)

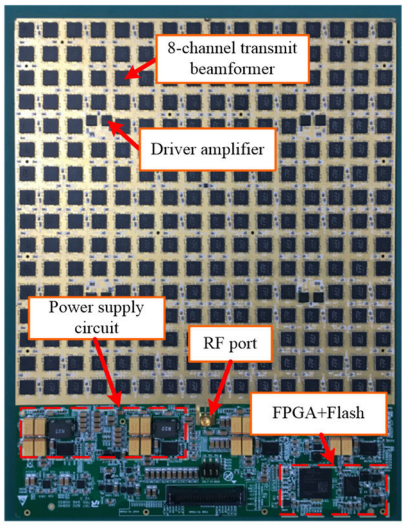

(b)

FIGURE 1. Top view (a) and bottom view (b) of the 1024-element transmit array.

phased arrays have become the most promising and practical ways to realize large arrays for the SATCOM terminals. The antenna based on CMOS and PCB tremendously reduce the cost of active phased arrays [23], [24]. However, most reports about silicon-based phased arrays focus on Ku-band SATCOM applications. To the best of the author's knowledge, there is only one paper, published by the University of California San Diego (UCSD) [19], about a dual-polarized 256-element Ka-band transmit array for SATCOM applications; the array can achieve a wide-angle scan in only one dimension (1D). Therefore, current research on silicon-based arrays for Ka-band SATCOM is far from a practical solution for commercial applications. There are some challenges that need to be taken into consideration, such as:

1. The aperture of the array is not large enough. The largest array has 256 (16 × 16) elements in current reports. However, from the regulation of European Telecommunications Standards Institute (ETSI), the phased array should be

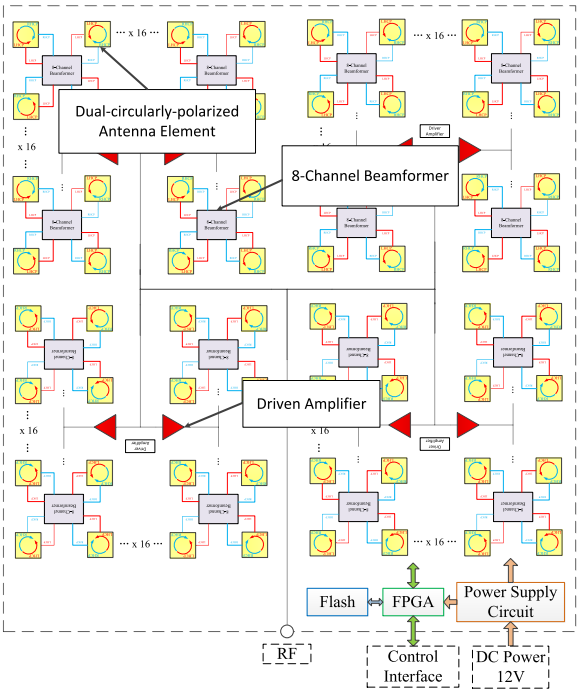

FIGURE 2. The radio architecture of the 1024-element transmit phased array.

a 4096-element (64 × 64) array or larger [20]. Although the scalable array can create an array with larger aperture, building the scalable array with small aperture not only increases the complexity and difficulty of assembly, but also causes the problem of flatness of the larger array. Furthermore, the radiation pattern of the SATCOM terminal antenna in any azimuth plane must comply with the regulations released by international organizations. However, due to the 2 × N scaling configuration, the 256-element (16 × 16) subarray can only realize (2 × 16) × (N × 16) elements array. Therefore, if we align 2 × 16 elements in the × direction and N × 16 elements in the Y direction, the beamwidth in XZ plane is not always narrow enough to comply with the regulations.

2. Due to the cost and manufacturability of the beamformer chips, the Si-based beamformer chips always integrate several channels with identical functions in a very compact size. In such design, the coupling between adjacent channels of the beamformer is significantly increased. This is a common problem for the silicon-based phased arrays. However, few of the current studies focus on the effect caused by the beamformer.

To the best of our knowledge, the 1024-element Ka-band transmit phased array is the largest scalable phased array for Ka-band SATCOM in recent reports, as shown in Fig. 1. The phased array can achieve a wide-angle (±60°)scan in two-dimension (2D). By applying the single-channel circular polarization architecture, the polarization of the array can swiftly switch between LHCP and RHCP modes. The axial ratio (AR) of the array at the boresight from 29.5GHz to 30GHz is lower than 2 dB. With the 8-channel transmit beamformer, the EIRP of the array can achieve 74 dBm at the bandwidth of interest. Moreover, the variation of the AR

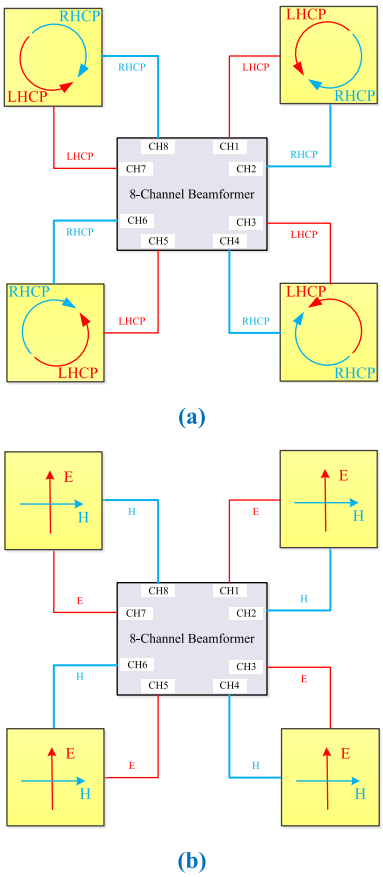

FIGURE 3. Architectures of (a) single channel circular polarization and (b) dual-channel circular polarization.

caused by the mutual coupling between adjacent channels is discussed in this work as well.

Section II introduces the radio architecture of the 1024-element transmit phased array. This section also compares the difference between the architecture of single channel circular polarization applied in this work and the architecture of dual channel circular polarization introduced by other reports. Section III presents the architecture of the 8-channel transmit CMOS beamformer and the performance of the chip. The channel-to-channel coupling effect is also discussed in this section. Section IV briefly presents the design of the multilayer PCB and the design of the dual-circularly-polarized antenna element. Section V introduces the calibration and measurement results of the 1024-element transmit array.

II. PHASED ARRAY ARCHITECTURE

A. ARCHITECTURE OF THE 1024-ELEMENT PHASED ARRAY

As shown in Fig. 2, the transmit phased array consists of 8-channel transmit beamformers, driver amplifiers, FPGA, FLASH, and the power supply circuit. The FPGA and FLASH act as an antenna control unit (ACU), which controls the function of beam-steering. Due to the insertion loss of the feeding network, we applied 8 pieces of driver amplifiers to mitigate the loss.

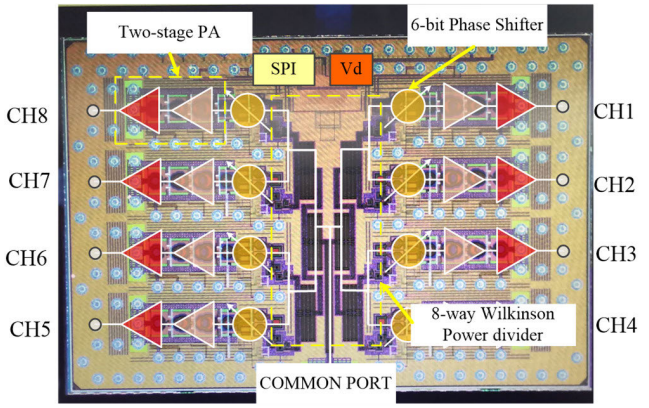

FIGURE 4. Architecture of the 8-channel transmit beamformer.

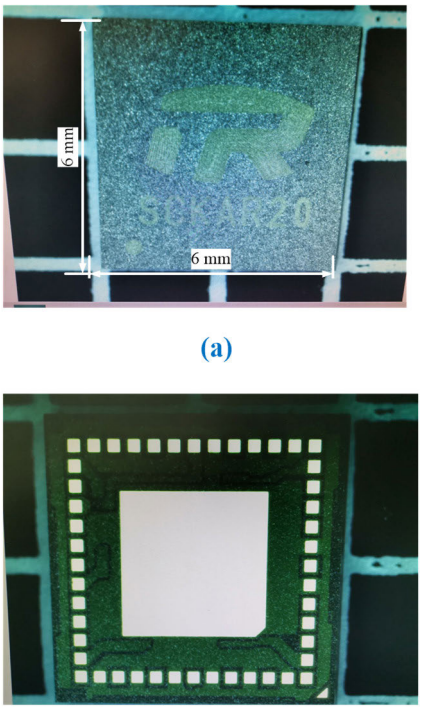

FIGURE 5. Chip in FC-LGA package: (a) top view and (b) bottom view.

All these devices are mounted on the multilayer PCB by Surface-mount Technology (SMT), as shown in Fig. 1(b). The multilayer PCB not only integrates the passive radio frequency (RF) circuits such as the dual-polarized antenna element and the feed network, but also integrates the network for signal and power distribution.

The size of the array is 160 mm × 210 mm. To avoid grating lobes in the scanning range of ±60°, the space of each antenna element is set to 5 mm × 5 mm.

B. ARCHITECTURE OF CIRCULAR POLARIZATION

It is well known that High Throughput Satellites (HTS) and some LEO constellations, such as the Telesat, adopt the polarization-division multiplexing method to increase the throughputs. Thus, the function of switchable

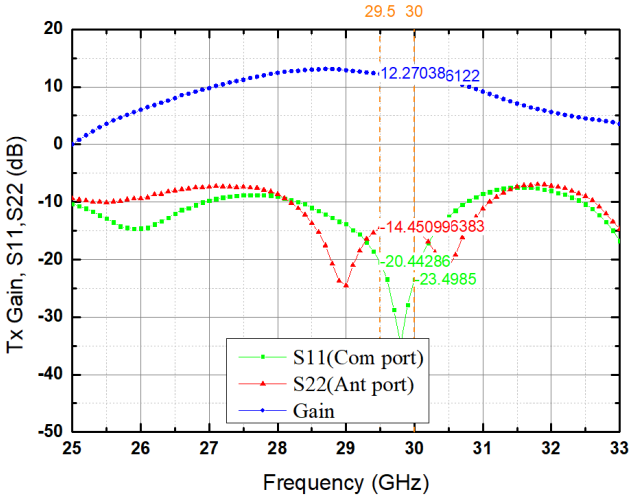

FIGURE 6. Measured S-parameter of the 8-channel beamformer.

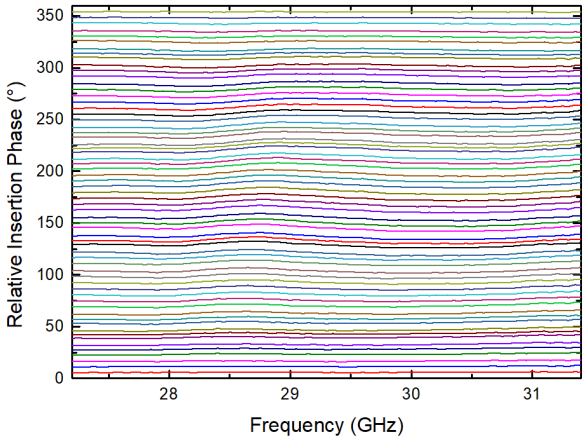

FIGURE 7. Measured relative insertion phase of the 8-channnel transmit beamformer.

TABLE 1. Measured 8-channel transmit beamformer performance.

PARAMETER	TYPICAL VALUE	UNIT
Frequency	29.5~30	GHz
Gain	12	dB
OP1dB	11	dBm
RMS phase error	4	deg
PDC per channel	75	mW

dual-circular polarization is a mandatory function for satellite terminals.

In most of recent reports, researchers applied dual channel circular polarization architectures to realize dual-circularly polarized antenna, as shown in Fig. 3(b). In this architecture, every dual-circularly-polarized antenna element is served by two channels of the beamformer simultaneously. With such architecture, the array theoretically can realize arbitrary polarization. However, for practical applications, this architecture has two defects: First, the number of channels of the beamformers controlled by the ACU is twice the number of

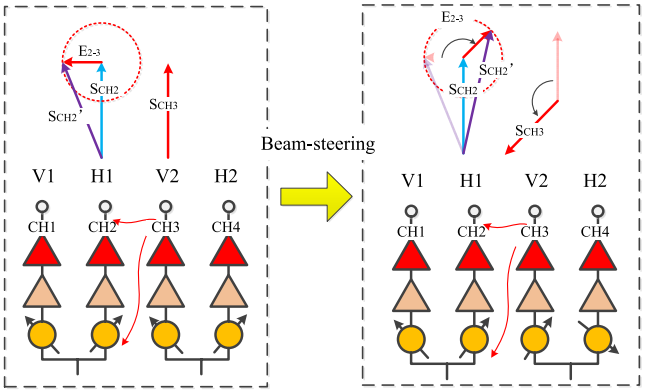

FIGURE 8. Coupling effect between adjacent channels.

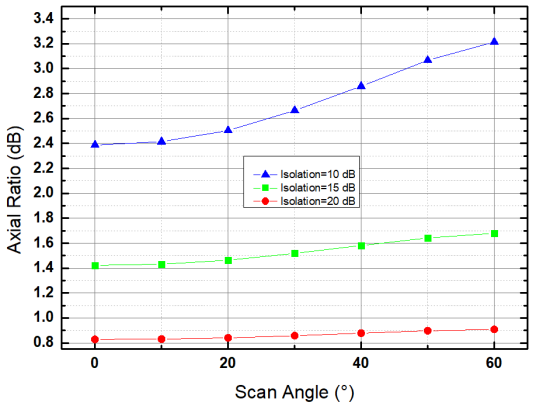

FIGURE 9. The variation in the axial ratio caused by beam steering.

the antenna elements. Thus, the time spent on the phase shift calculation is increased and the speed of beam-steering is consequently decreased. For large array or high-speed platform, such as jet aircraft, this problem cannot be neglected. Second, as we mentioned before, there is mutual coupling between the channels of the beamformer. In dual channel circular polarization architecture, when the beam is steering, the coupling can cause variation of the axial ratio (AR) of the antenna element. This problem is elaborately discussed in Section III. Therefore, we applied single-channel circular polarization architecture, as shown in Fig. 3(a).

In single channel architecture, each channel of the beamformer can independently excite the antenna to radiate circular polarization electromagnetic wave. For example, the CH1 of the 8-channel beamformer can drive the antenna element to generate LHCP waves as shown in Fig. 3(a). By contrast, the CH1 of the dual channel architecture can only generate linearly polarized waves in the E-plane.

III. 8-CHANNEL CMOS TRANSMIT BEAMFORMER

The 8-channel CMOS beamformer chip is fabricated by the TSMC's 65 nm CMOS process and the architecture of transmit beamformer is shown in Fig. 4.

As shown in Fig. 4, the 8-channel beamformer consists of 8 independent RF channels, an 8-way Wilkinson feed network and the interface circuit of SPI. The Wilkinson feed

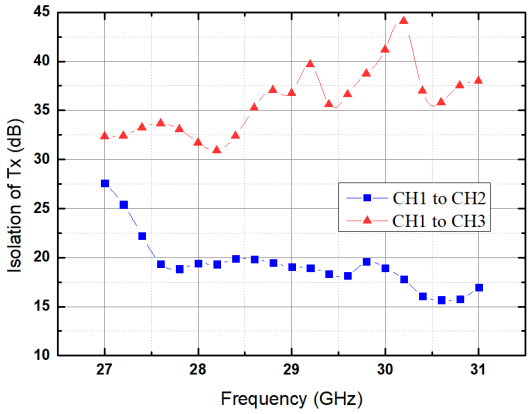

FIGURE 10. Measured channel to channel isolation between adjacent and alternating channels.

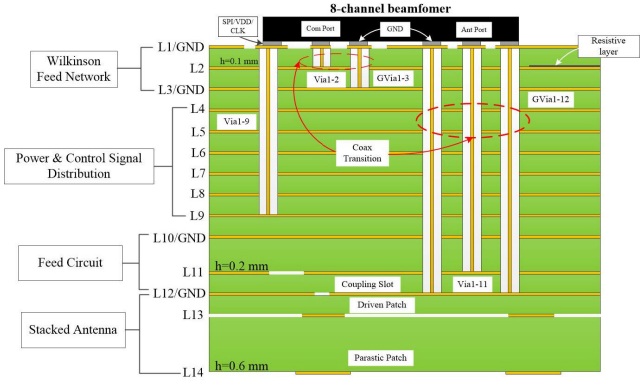

FIGURE 11. Multilayer PCB stackup.

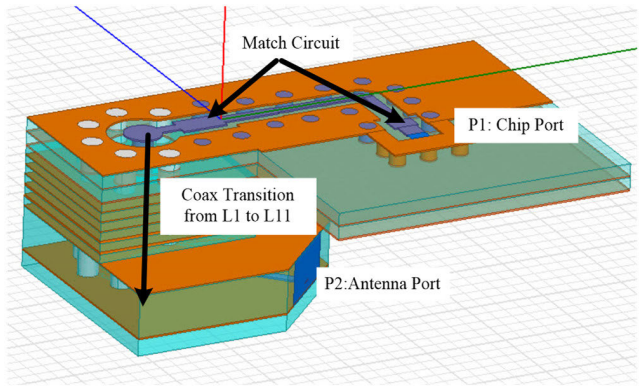

FIGURE 12. Coax Transition circuit of (a) Tx and (b) Rx.

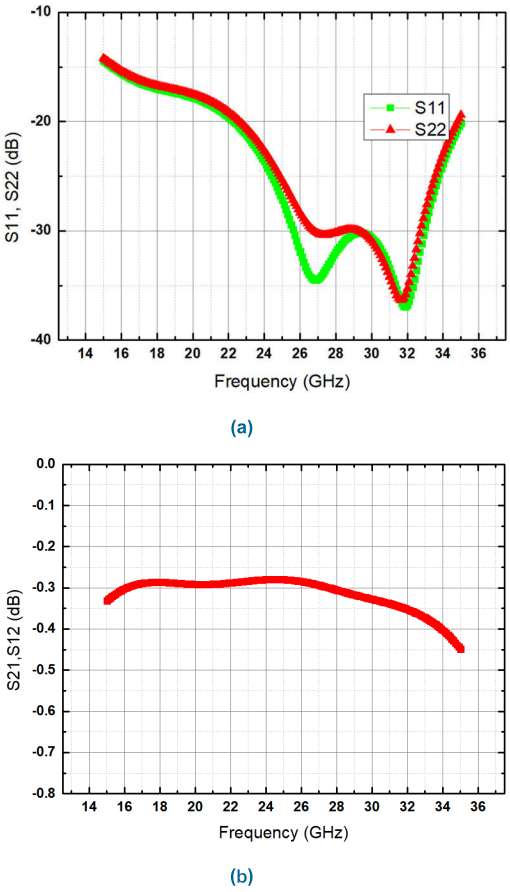

FIGURE 13. Simulated S-parameter of the coax transition circuit.

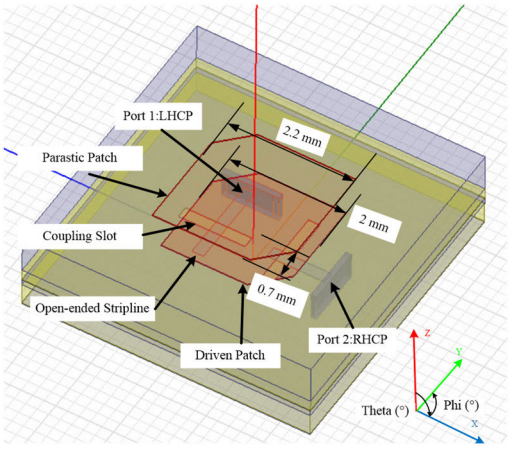

FIGURE 14. Dual-circularly polarized antenna element.

network evenly distributes the input signal to each RF channel. Each RF channel consists of a two-stage power amplifier and a 6-bit phase shifter. The phase shifter in each channel is based on the architecture of an analog reflection-type passive vector modulator, which has a compact size and zero power consumption.

As shown in Fig. 5, the transmit beamformer applies plastic package.

The measured S-parameter of the 8-channel beamformer is illustrated in Fig. 6. The operating band of the transmit beamformer is from 27 GHz to 31 GHz.

The phase shifting measurement result is shown in Fig. 7.

Other measured results of the packaged beamformer chip are summarized in Table 1.

In addition to the parameters discussed above, for the phased array design, it is essential to consider the channel-to-channel coupling of the beamformer chip.

In the dual channel circular polarization architecture, the CH1 and CH2 excite two orthogonal linearly-polarized signals (V1, H1) for the antenna element 1, respectively.

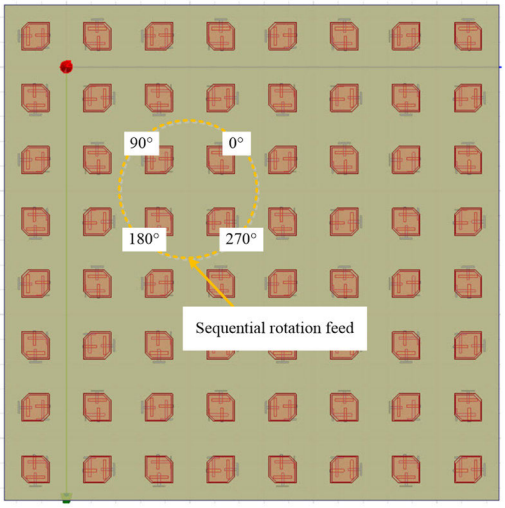

FIGURE 15. Simulation model of an 8 × 8-element array.

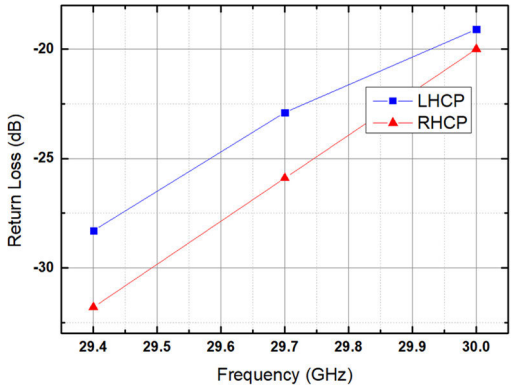

FIGURE 16. Simulation results of reflection loss of the antenna element.

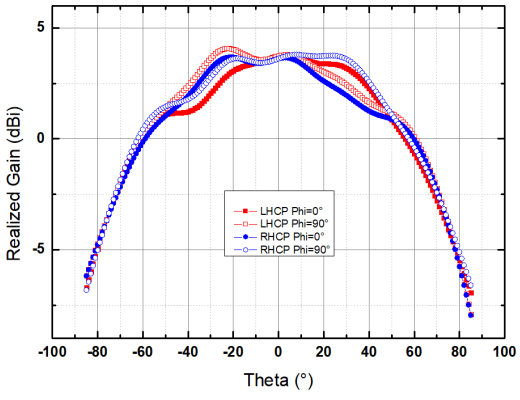

FIGURE 17. Simulated antenna pattern at 29.7GHz.

Ideally, the phase difference of CH1 and CH2 is ±90 degree. However, as shown in Fig. 8, due to the mutual coupling between CH2 and CH3, the output signal of CH2 become S_{CH2}', the composite vector of the desired signal, S_{CH2}, and the error signal caused by CH3, E_{2-3}. Moreover, CH3 and CH4, serving antenna element 2, change their phase when the array steers the beam off the boresight. Consequently, the

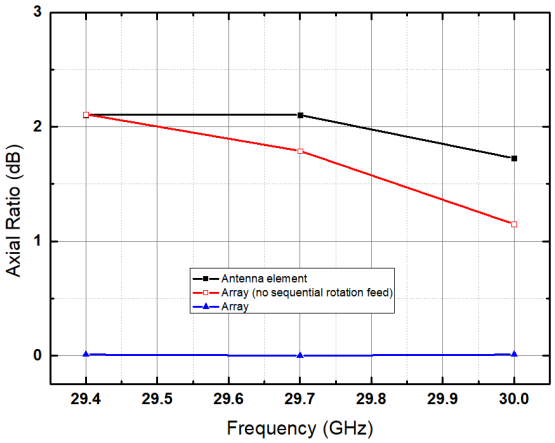

FIGURE 18. Simulated AR of the single element and 8 × 8 array.

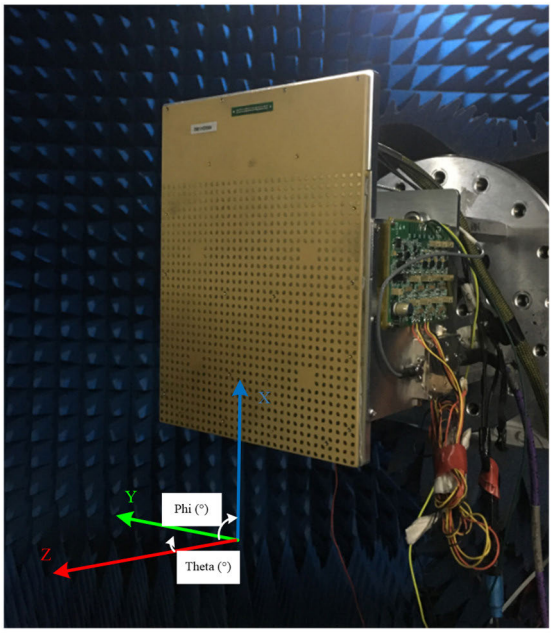

FIGURE 19. The 1024-element transmit phased array tested in anechoic chamber.

composite vector S_{CH2}' changes and the axial ratio of antenna element 1 also changes with the scan angle, as shown in Fig. 8. The method to calculate the axial ratio considering the effect of errors is introduced in [25].

As shown in Fig. 9, the AR increases as the beam scans at larger angles. When the isolation between CH2 and CH3 decreases to 10 dB, the variation in the axial ratio becomes more obvious. Theoretically, an improved AR can be achieved by calibration [26]. However, it is impossible to calibrate the AR of the array for every scan angle considering the calibration time. Therefore, it is reasonable to choose single channel circular polarization architecture to avoid the effect of channel-to-channel coupling on the axial ratio of the array. In the single channel architecture, the mutual coupling has no influence on the axial ratio of antenna, which is determined by antenna type. However, the coupling among channels can still affect the radiation pattern of the array in

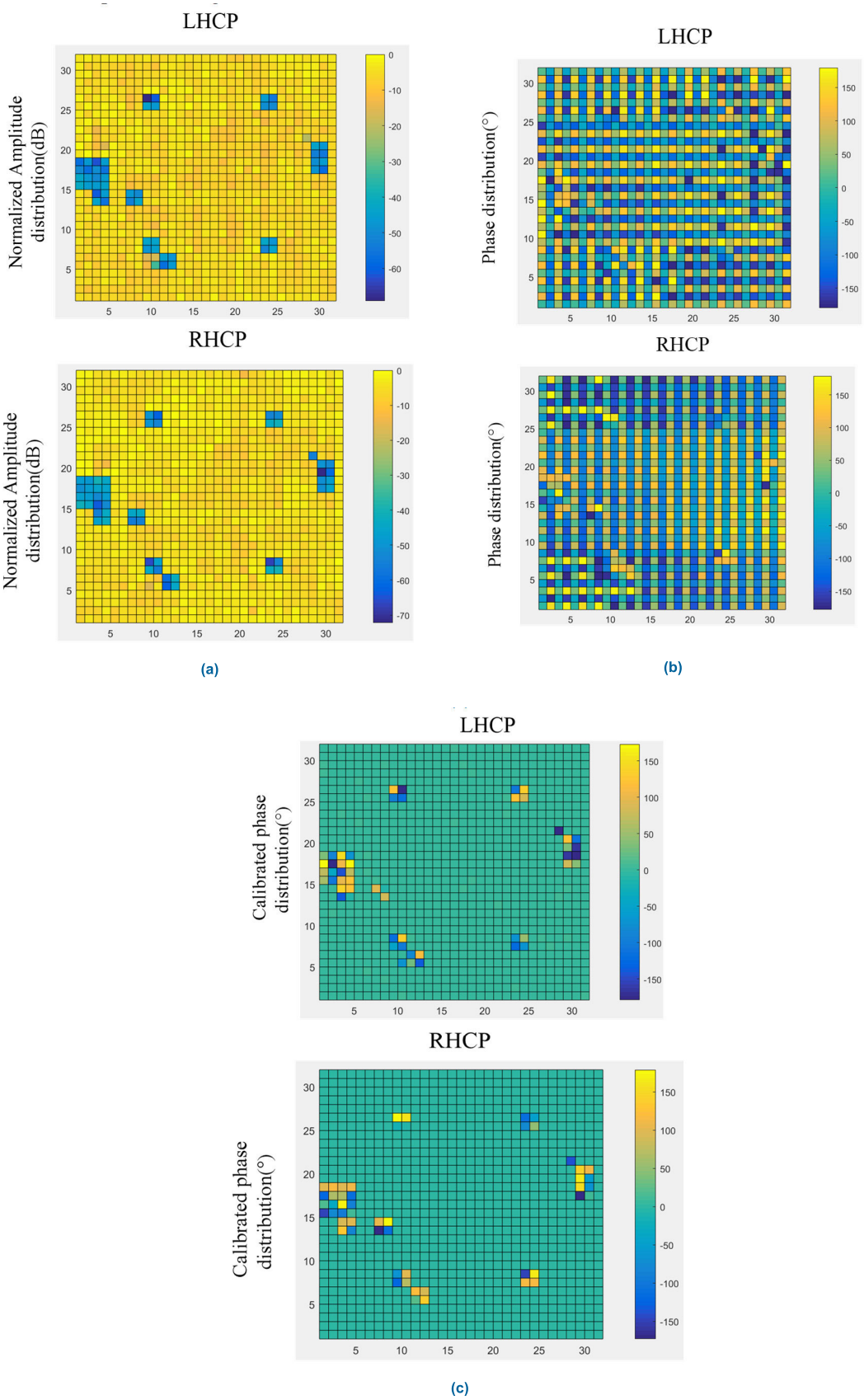

FIGURE 20. Measured (a) amplitude distribution, (b) phase distribution of transmit array in LHCP and RHCP modes at 29.7 GHz and the (c) phase distribution after calibration.

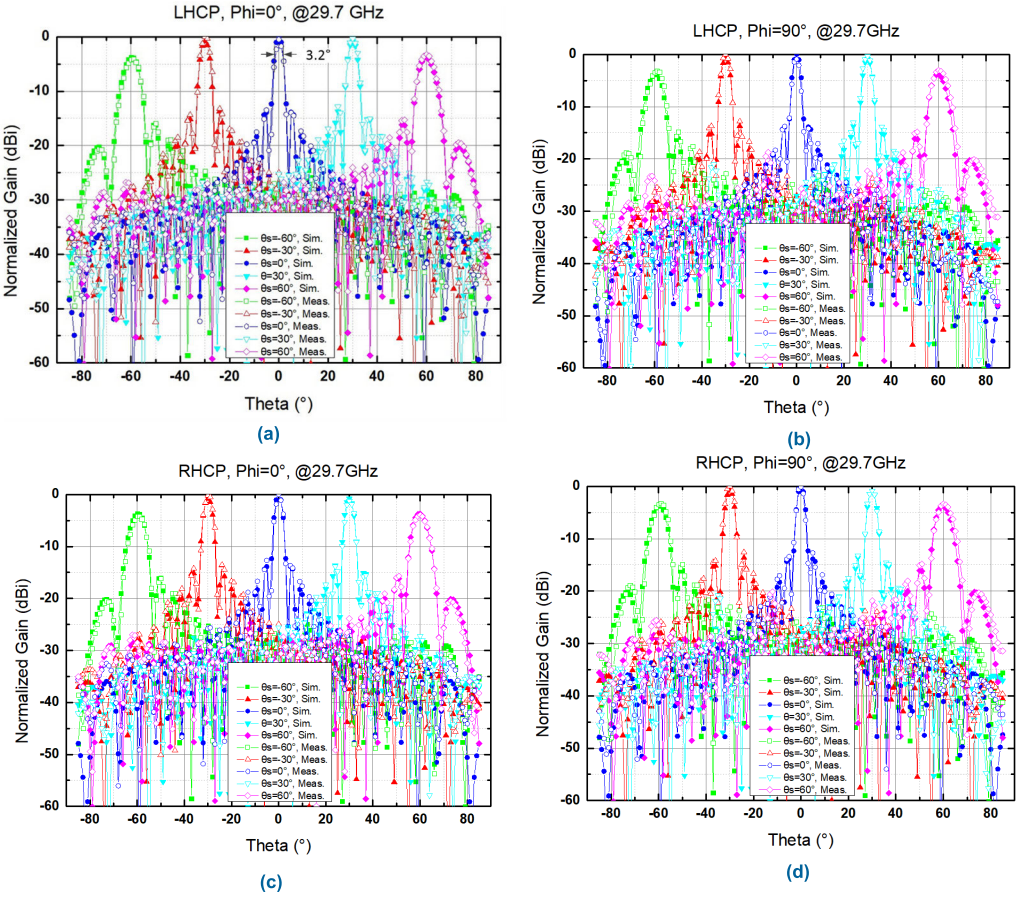

FIGURE 21. Measured and simulated radiation pattern of the 1024-element array in (a) LHCP mode in the phi = 0° plane (YZ-plane), (b) LHCP mode in the phi = 90° plane (XZ-plane), (c) RHCP mode in the phi = 0° plane, (d) RHCP mode in the phi = 90° plane.

both the single and dual channel architectures. Thus, it is essential to keep the channel to channel isolation at a high level (č¿20 dB). In this design, due to the architecture applied, no adjacent channel needs to work at the same time and the channel-to-channel isolation between alternating channels is high enough to achieve a desirable radiation pattern, as shown in Fig. 10.

It is obvious that the isolation between adjacent channels is much lower than that between the alternating channels.

IV. THE DESIGN OF MULTILAYER PCB AND DUAL-CIRCULARLY-POLARIZED ANTENNA ELEMENT

The multilayer PCB applies Panasonic Megtron-6 ($\varepsilon_r = 3.3, tan\delta = 0.005\ at\ 30GHz$) as a substrate material and integrates four circuits: the 1:256 Wilkinson feed network, the network for power and digital signal distribution, the feed circuit for the antenna element and the stacked patch antenna. As shown in Fig. 11, the beamformer chip is mounted on L1, and its common port connects with the Wilkinson feed network by Via1-2. Then, the antenna ports of the beamformer transmit the RF signal from the antenna element through the coaxial vias, which consist of Via1-11 and GVia1-12. Other signals of the beamformer, such as SPI and the power supply, are distributed from L4 to L9 through Via1-9.

A. PASSIVE CIRCUIT SIMULATION

The coax transition circuits between the beamformer chip and the feed circuit of antenna are shown in Fig. 12 and the match circuits are used to improve the bandwidth of the coax transition.

The simulation results are illustrated in Fig. 13. The S11 and S22 of the coax transition circuit from 22 GHz to 34 GHz are less than -20 dB, and the insertion loss is less than -0.32 dB at the bandwidth of interest.

B. ANTENNA ELEMENT DESIGN AND SIMULATION

As shown in Fig. 14, the dual-circularly-polarized antenna in this work is an aperture-coupled stacked patch antenna and implemented by 5 metal layers from L10 to L14. The feed circuit is built in L11 and excites the driven patch in L13 through the coupling slot in L12. The parasitic patch in L14 can increase the bandwidth. Moreover, the thickness of the substrate between the driven patch and the parasitic patch is increased to widen the antenna bandwidth.

However, due to the narrow element space (5 mm × 5 mm) of the array and the limitation of PCB design rules, the single-fed configuration is a feasible solution, as shown in Fig. 13. The driven and parasitic patches are trimmed to realize circular polarization. Two orthogonal coupling slots and the related open-ended striplines connect with adjacent channels

of the beamformer. Therefore, the antenna can switch from LHCP to RHCP mode, when the signal switches from port 1 to port 2.

Furthermore, the transmit array applies the sequential rotation feeding method to improve the AR of the array. Moreover, considering the mutual coupling effects between adjacent antennas, we simulate the single element in the middle of an 8 × 8 elements array, as shown in Fig. 15.

The simulated reflection loss of the antenna element is illustrated in Fig. 16.

The simulated reflection loss of the antenna element in RHCP and LHCP modes are both below −20 dB.

As shown in Fig. 17, due to the mutual coupling effect, the radiation patterns of the antenna element are not symmetric in the Phi = 0° plane or the Phi = 90° plane. The simulated antenna gain is approximately 4 dBi at 29.7 GHz.

Due to applying the sequential rotation feeding method, the AR of the array is significantly improved. The comparison of simulated AR between the single antenna element and the array is illustrated in Fig. 18.

V. MEASUREMENT OF THE 1024-ELEMENT TRANSMIT PHASED ARRAY

As shown in Fig. 19, the 1024-element phased array is calibrated and measured in a far field anechoic chamber by using a vector network analyzer. The amplitude and phase distribution of the array in LHCP and RHCP modes at 29.7 GHz are plotted in Fig. 20.

From the amplitude distribution and the calibrated phase distribution of the 1024-element array in Fig. 20, we found that a few channels fail to work other than the channels removed for providing space for driven chips. The welding defects from the SMT process are the main cause of this problem. Moreover, the defects also cause the variation of amplitude distribution of the array. The measured amplitude variation of the array is approximately 10 dB. After phase calibration, the phase variations of the array is less than 4° except for the failed channels.

The measured and simulated radiation patterns of the transmit array in LHCP and RHCP modes at 29.7 GHz for different scan angle (theta) are shown in Fig. 21.

The measurement shows that the array can steer over the scan angles from −60° to 60° in both the Phi = 0° (YZ) and Phi = 90° (XZ) plane. In LHCP mode, the beamwidth of the array at boresight in both the Phi = 0° (YZ) plane and the Phi = 90° (XZ) plane are 3.2°. The sidelobe is lower than -10 dB over all scan angles. In RHCP mode, the beamwidth at boresight in both the Phi = 0° (YZ) and Phi = 90° (XZ) plane are also 3.2° with sidelobes <-10 dB over all scan angles. The measured radiation patterns of the Tx array agree with the simulation results and the radiation patterns in LHCP and RHCP mode are identical. The gain of the array decreases by 4 to 4.5 dB as the beam scans at ±60°, as shown in Fig. 21.

As shown in Fig. 22, the measured AR of the array at the boresight are lower than 2 dB in both LHCP and RHCP mode

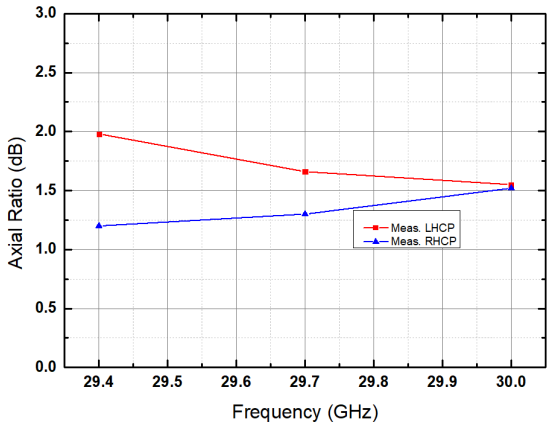

FIGURE 22. Measured AR of the 1024-element transmit array at the boresight in LHCP and RHCP modes.

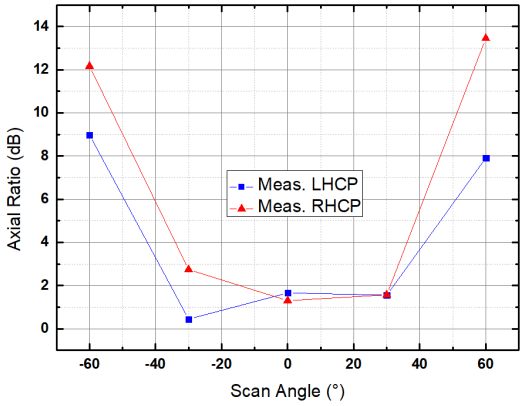

FIGURE 23. Measured axial ratio of the array with different scan angles at 29.7 GHz.

at the bandwidth of interest. Due to the single channel circular polarization, the 10 dB amplitude variation of the array has no effect on the AR of the array.

As shown in Fig. 23, the AR of the array is increased to 12 dB when the array scans to large angle. The significant deterioration of the array's AR can be caused by two reasons. First, as we know, the single-fed antenna element has narrow circular polarization (CP) beamwidth. Second, although we apply the sequential rotation feeding method to improve the AR of the array, the mutual coupling effect at large scan angles increases the variations of amplitude and phase. Thus, the amplitude and phase of each channel are not ideal as expected.

In addition to the radiation pattern and the AR of the phased array, the EIRP of transmit array is one of the most important parameters for SATCOM applications and, decides the link budget of the return link (RTN) of SATCOM. The EIRP can be roughly estimated by the link calculation before measurement. The method of link calculation is thoroughly introduced in [27]. In the link calculation, the phase and amplitude distribution of the array is assumed to be uniform. From the link calculation, the EIRP of the array at the boresight is approximately 75 dBm. However, due to the defects

TABLE 2. Performance comparison with Prior Articles.

	This work	UCSD [14]	UCSD [19]	IBM [15]	C-COM [21]
Process	65 nm CMOS	0.18 μm SiGe BiCMOS	SiGe BiCMOS	0.13 μm SiGe BiCMOS	Not mentioned
Frequency (GHz)	29.5~30	28-32	28-30	26.5~29.5	27.5-31
No. of elements in array	32 x 32 Tx	8 x 8 TRx	16 x 16 Tx	8 x 8 TRx	16 x 16 Tx
Scaling design	Yes	No	Yes	Yes	Yes
Scan angle in Phi=0° and Phi=90° plane (°)	±60/±60	±25/±50	±5/±60	±50/±50	±70/±70
Side lobe (dB)	< -10	< -10	< -13	< -10	< -10
Polarization	Dual Circularly-Polarized (CP)	Single Linearly-Polarized (LP)	Dual CP	Dual LP	Single CP
Axial ratio at the boresight (dB)	2	--	6	--	Not mentioned
EIRP at OP1dB (dBm)	74	52	64.5	54	64.5
Output power of each channel (dBm)	11	11-12	10	Not mentioned	10-12

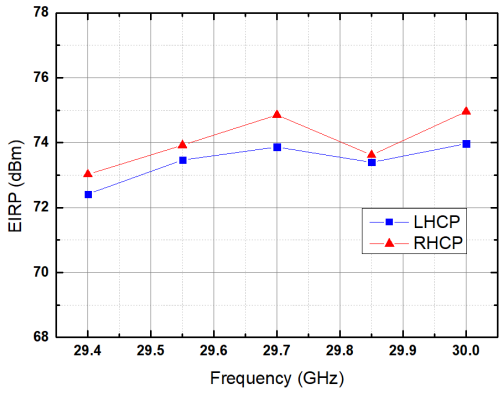

FIGURE 24. Measured EIRP of the 1024-element Tx array.

caused by the SMT process, a few channels of the array with lower gain failed to output enough power. Therefore, the array cannot achieve the expected EIRP, which is determined by the total transmit power. With the influence of the amplitude variation, the measured EIRP is almost 1 dB lower than the calculation result, as shown in Fig. 24.

The power consumption of the 1024-element transmit array at OP1dB (output 1-dB compression point) is 108W. The measured power consumption includes the power consumption of the RF chips (beamformers and driven chips), ACU and power supply circuit. Finally, with 10W total transmit power, the efficiency of the array is approximately 9.3%.

As shown in Table 2, the phased array in this work has the largest number of channels and achieves the highest EIRP in comparison with prior arts. Furthermore, the cost of the CMOS process applied in this work is much less than the SiGe BiCMOS process applied in the other works. Therefore, the phased array in our research is much more practical for mass production and commercial application.

VI. CONCLUSION

This paper presents a scalable 1024-element transmit dual-circularly-polarized planar phased array. The design and measured results of the array are thoroughly introduced in this paper. The array consists of 8-channel beamformers and a multilayer PCB. With the single channel circular polarization architecture, the array can easily realize switchable dual circular polarization. According to the measurement results, the array can steer up to ±60° off the boresight without any grating lobes. The EIRP of the array can achieve almost 74 dBm in both LHCP and RHCP mode from 29.5 GHz to 30 GHz. Compared with the prior art, the measurement results demonstrate that the transmit phased array based on CMOS and PCB technology is a feasible solution for SATCOM terminals applied in GEO and LEO system.

ACKNOWLEDGMENT

The authors would like to thank Chengdu T-Ray Technology Company Ltd., for generously providing the beamformer chips and Dr. Z.-H. Chen, the CTO of Chengdu T-Ray

Technology Company Ltd., for technical support. The authors would also like to thank other colleagues from the Chengdu T-Ray Technology Company Ltd., for making this project possible.

REFERENCES

[1] *5 Trends in Satellite Communications on the Horizon*. Accessed: Aug. 7, 2018. [Online]. Available: https://news.itu.int/satellite-communications-trends/

[2] M. Abo-Zeed, J. B. Din, I. Shayea, and M. Ergen, "Survey on land mobile satellite system: Challenges and future research trends," *IEEE Access*, vol. 7, pp. 137291–137304, 2019.

[3] *A Year of Evolution: Top 5 Satellite Trends in 2018*. Accessed: Dec. 20, 2018. [Online]. Available: https://www.satellitetoday.com/business/2018/12/20/a-year-of-evolution-top-5-satellite-trends-in-2018/

[4] H. Fenech, S. Amos, A. Tomatis, and V. Soumpholphakdy, "High throughput satellite systems: An analytical approach," *IEEE Trans. Aerosp. Electron. Syst.*, vol. 51, no. 1, pp. 192–202, Jan. 2015.

[5] K. T. Pham, A. Clemente, E. Fourn, F. Diaby, L. Dussopt, and R. Sauleau, "Low-cost metal-only transmitarray antennas at ka-band," *IEEE Antennas Wireless Propag. Lett.*, vol. 18, no. 6, pp. 1243–1247, Jun. 2019, doi: 10.1109/LAWP.2019.2913571.

[6] S. A. Matos, E. B. Lima, J. S. Silva, J. R. Costa, C. A. Fernandes, N. J. G. Fonseca, and J. R. Mosig, "High gain dual-band beam-steering transmit array for satcom terminals at ka-band," *IEEE Trans. Antennas Propag.*, vol. 65, no. 7, pp. 3528–3539, Jul. 2017, doi: 10.1109/TAP.2017.2702658.

[7] T. Chaloun, M. Kaynak, W. Menzel, Q. Luo, T. Purtova, S. Gao, V. Ziegler, H. Schumacher, F. Tabarani, and R. Starec, "Wide-angle scanning active transmit/receive reflectarray," *IET Microw., Antennas Propag.*, vol. 8, no. 11, pp. 811–818, Aug. 2014, doi: 10.1049/iet-map.2013.0704.

[8] A. Mehdipour, M. Sazegar, and R. Stevenson, "Broadband WAIM metasurface structure for electronically beam scanning holographic antenna for ku-band satellite communications," in *Proc. IEEE Int. Symp. Antennas Propag. USNC-URSI Radio Sci. Meeting*, Atlanta, GA, USA, Jul. 2019, pp. 429–430.

[9] O. H. Karabey, A. Gaebler, S. Strunck, and R. Jakoby, "A 2-D electronically steered phased-array antenna with 2×2 elements in LC display technology," *IEEE Trans. Microw. Theory Techn.*, vol. 60, no. 5, pp. 1297–1306, May 2012, doi: 10.1109/TMTT.2012.2187919.

[10] B. Sadhu, X. Gu, and A. Valdes-Garcia, "The more (Antennas), the merrier: A survey of silicon-based mm-wave phased arrays using multi-IC scaling," *IEEE Microw. Mag.*, vol. 20, no. 12, pp. 32–50, Dec. 2019, doi: 10.1109/MMM.2019.2941632.

[11] L. Paulsen, M. Livadaru, E. Dobbins, J. Wolf, J. West, A. Walker, V. Olen, J. Reyland, C. Olson, and G. Rebeiz, "Fabrication and measurement of a large, monolithic, PCB-based AESA," in *Proc. IEEE Int. Symp. Phased Array Syst. Technol. (PAST)*, Waltham, MA, USA, Oct. 2016, pp. 1–7.

[12] G. M. Rebeiz and L. M. Paulsen, "Advances in SATCOM phased arrays using silicon technologies," in *IEEE MTT-S Int. Microw. Symp. Dig.*, Honolulu, HI, USA, Jun. 2017, pp. 1877–1879.

[13] H. Al-Saedi, W. M. Abdel-Wahab, S. M. Raeis-Zadeh, E. H. M. Alian, A. Palizban, A. Ehsandar, N. Ghafarian, G. Chen, S. Rasti Boroujeni, M.-R. Nezhad-Ahmadi, and S. Safavi-Naeini, "An integrated circularly polarized transmitter active phased-array antenna for emerging ka-band satellite mobile terminals," *IEEE Trans. Antennas Propag.*, vol. 67, no. 8, pp. 5344–5352, Aug. 2019.

[14] K. Kibaroglu, M. Sayginer, T. Phelps, and G. M. Rebeiz, "A 64-element 28-GHz phased-array transceiver with 52-dBm EIRP and 8–12-Gb/s 5G link at 300 meters without any calibration," *IEEE Trans. Microw. Theory Techn.*, vol. 66, no. 12, pp. 5796–5811, Dec. 2018, doi: 10.1109/TMTT.2018.2854174.

[15] X. Gu, D. Liu, C. Baks, O. Tageman, B. Sadhu, J. Hallin, L. Rexberg, P. Parida, Y. Kwark, and A. Valdes-Garcia, "Development, implementation, and characterization of a 64-element dual-polarized phased-array antenna module for 28-GHz high-speed data communications," *IEEE Trans. Microw. Theory Techn.*, vol. 67, no. 7, pp. 2975–2984, Jul. 2019.

[16] A. H. Aljuhani, E. Traffenstedt, T. Kanar, S. Zihir, and G. M. Rebeiz, "Ultra-low cost ku-band dual-polarized transmit and receive phased-arrays for SATCOM and Point-to-Point applications with bandwidths up to 750 MHz," in *Proc. IEEE Int. Symp. Phased Array Syst. Technol. (PAST)*, , MA, USA, Oct. 2019, pp. 8138–8143.

[17] W. Theunissen, V. Jain, and G. Menon, "Development of a receive phased array antenna for high altitude platform stations using integrated beamformer modules," in *IEEE MTT-S Int. Microw. Symp. Dig.*, Jun. 2018, pp. 779–782.

[18] A. I. Sandhu, E. Arnieri, G. Amendola, L. Boccia, E. Meniconi, and V. Ziegler, "Radiating elements for shared aperture Tx/Rx phased arrays at K/Ka band," *IEEE Trans. Antennas Propag.*, vol. 64, no. 6, pp. 2270–2282, Jun. 2016, doi: 10.1109/TAP.2016.2552550.

[19] K. K. Wei Low, A. Nafe, S. Zihir, T. Kanar, and G. M. Rebeiz, "A scalable circularly-polarized 256-element ka-band phased-array SATCOM transmitter with ±60◦ beam scanning and 34.5 dBW EIRP," in *IEEE MTT-S Int. Microw. Symp. Dig.*, Boston, MA, USA, Jun. 2019, pp. 1064–1067, doi: 10.1109/MWSYM.2019.8701112.

[20] T. Lambard, O. Lafond, M. Himdi, H. Jeuland, S. Bolioli, and L. Le Coq, "Ka-band phased array antenna for high-data-rate SATCOM," *IEEE Antennas Wireless Propag. Lett.*, vol. 11, pp. 256–259, 2012, doi: 10.1109/LAWP.2012.2189747.

[21] W. M. Abdel-Wahab, H. Al-Saedi, E. H. Mirza Alian, M. Raeis-Zadeh, A. Ehsandar, A. Palizban, N. Ghafarian, G. Chen, H. Gharaee, M. R. Nezhad-Ahmadi, and S. Safavi Naeini, "A modular architecture for wide scan angle phased array antenna for K/Ka mobile SATCOM," in *IEEE MTT-S Int. Microw. Symp. Dig.*, Boston, MA, USA, Jun. 2019, pp. 1076–1079, doi: 10.1109/MWSYM.2019.8700842.

[22] A. H. Aljuhani, T. Kanar, S. Zihir, and G. M. Rebeiz, "A scalable dual-polarized 256-element Ku-band phased-array SATCOM receiver with ±70◦ beam scanning," in *IEEE MTT-S Int. Microw. Symp. Dig.*, Philadelphia, PA, USA, 2018, pp. 1203–1206, doi: 10.1109/MWSYM.2018.8439257.

[23] M. G. Livadaru, *Low Cost Scanning Arrays*. Miami, FL, USA: Florida International Univ., 2018.

[24] L. Coryell, R. Hoffman, R. Lau, and J. Shields, "The long road to affordable phased arrays," in *Proc. Allerton*, Allerton, IL, USA, 2010, pp. 1–9.

[25] S. V. Parekh, "Simple formulae for circular-polarization axial-ratio calculations," *IEEE Antennas Propag. Mag.*, vol. 33, no. 1, pp. 30–32, Feb. 1991, doi: 10.1109/74.80660.

[26] M. A. Salas-Natera, R. Martínez Rodríguez-Osorio, L. Y. de Haro Ariet, and M. Sierra Pérez, "Circularly polarized active antenna array system calibration for improved axial ratio systems," in *Proc. 13th Eur. Conf. Antennas Propag. (EuCAP)*, Krakow, Poland, 2019, pp. 1–5.

[27] X. Luo, J. Ouyang, Z. Chen, L. Han, and W. Yan, "A low-profile 36-element K-Band active phased array for ultra-small aperture application," *IEEE Access*, vol. 8, pp. 62286–62297, 2020, doi: 10.1109/ACCESS.2020.2983604.

XUAN LUO (Associate Member, IEEE) received the M.Sc. degree in electromagnetic field and microwave technology from the University of Electronic Science and Technology of China (UESTC), in 2011, where he is currently pursuing the Ph.D. degree. He is also an RF Engineer with Chengdu T-Ray Technology Company Ltd. His research interests include SATCOM, 5G communication, phased array antenna, and mm-wave T/R module.

JUN OUYANG received the Ph.D. degree in electromagnetic field and microwave technology and the Ph.D. degree in information and signal processing from the University of Electronic Science and Technology of China (UESTC), in 2008 and 2011, respectively. He is currently an Associate Professor with the School of Electronic Science and Engineering, UESTC, where he is an Associate Director with the Smart Cities Research Center. He is also a Research Fellow and the Chief Scientist of the Internet of Things technology with the Chengdu Research Institute. He is leading several national-level research projects and provisional and ministerial research projects. He is the author of more than 80 articles. He holds 20 patents. His research interests include antenna theory and design, microwave systems, RFID tag, wireless sensing, and the Internet of Things.

ZHI-HUI CHEN received the Ph.D. degree in electronics engineering from Xidian University, Xi'an, China, in 2007. He has 12 years' experience in active phased array antenna, synthesis of antenna arrays, and RF equipment of commercial telecommunication implementation of satellite communication systems. He is currently a CTO with Chengdu T-Ray Technology Company Ltd. His research interests include phased array antenna, antenna measurement, and satellite communication systems.

YI YAN (Member, IEEE) was born in Anhui, China, in 1991. He received the B.Sc. degree in electromagnetic field and microwave technique from the University of Electronic Science and Technology of China (UESTC), Chengdu, China, in 2014, where he is currently pursuing the Ph.D. degree with the School of Electronic Science and Engineering. He is the author of several peer-reviewed international journal and conference papers. His current research interests include the theory of characteristic modes and terminal antenna design for future wireless communication technologies.

LEI HAN received the B.E. and M.Sc. degrees in electromagnetic field and microwave technology from the University of Electronic Science and Technology of China (UESTC), in 2007 and 2010, respectively. He is currently pursuing the Ph.D. degree with Air Force Engineering University (AFEU). His research interests include wide-band phased array, conformal antenna, and microstrip antenna design.

ZUBING WU received the M.Sc. degree in electromagnetic field and microwave technology from the University of Electronic Science and Technology of China (UESTC), in 2011. He is currently an Antenna Engineer with Chengdu T-Ray Technology Company Ltd. His research interests include microstrip antenna design and phased array design.

TAO YU received the M.Sc. degree in circuits and system technology from the University of Electronic Science and Technology of China (UESTC), in 2012. He is currently an RF Engineer with Chengdu T-Ray Technology Company Ltd. His research interests include mm-wave T/R module and microwave circuit design.

KAI ZHENG received the M.Sc. degree in electromagnetic field and microwave technology from the University of Electronic Science and Technology of China (UESTC), in 2010. He is currently an Antenna Test Engineer with Chengdu T-Ray Technology Company Ltd. His research interests include antenna measurement and measurement system integration.